

We are IntechOpen, the world's leading publisher of Open Access books Built by scientists, for scientists

4,800

Open access books available

122,000

International authors and editors

135M

Downloads

Our authors are among the

154

Countries delivered to

TOP 1%

most cited scientists

12.2%

Contributors from top 500 universities



WEB OF SCIENCE™

Selection of our books indexed in the Book Citation Index
in Web of Science™ Core Collection (BKCI)

Interested in publishing with us?
Contact book.department@intechopen.com

Numbers displayed above are based on latest data collected.
For more information visit www.intechopen.com



Surface Plasmon Enhanced Chemical Reactions on Metal Nanostructures

Rajkumar Devasenathipathy, De-Yin Wu and Zhong-Qun Tian

Abstract

Noble metal nanomaterials as plasmonic photocatalysts can strongly absorb visible light and generate localized surface plasmon resonance (SPR), which in turn depends on the size, shape, and surrounding of the plasmonic metal nanomaterials (PMNMs). Remarkably, the high-efficiency conversion of solar energy into chemical energy was expected to be achieved by PMNMs. Therefore, researchers have chosen PMNMs to improve the photocatalytic activity toward targeted molecules. This enhancement can be achieved by the effective separation of photogenerated electrons and holes of the PMNMs in the presence of light. Surface-enhanced Raman spectroscopy (SERS) has been performed for obtaining information about the photochemically transformed surface species at molecular levels. A profound understanding of kinetic mechanisms is needed for the development of novel plasmonic catalysts toward various chemical transformations of targeted molecules. In this chapter, based on the above discussions, the participation of SPR excitation in PMNMs and photocatalysis toward chemical transformations of SERS-active organic molecules such as aromatic amino and nitro compounds based on PMNMs have been discussed in detail through theoretical and experimental studies. Eventually, a summary and the future directions of this study are discussed.

Keywords: plasmonic metal nanomaterials, surface plasmon resonance, surface-enhanced Raman scattering, chemical reaction, aromatic amino and nitro compounds

1. Introduction

Surface plasmon resonance (SPR) is the phenomenon resulting from the resonant oscillation of conduction electrons present at the interface between negative and positive permittivity of plasmonic metal nanomaterials (PMNMs) that can be induced by incident light. The electric field of the incident light and the free electrons present in PMNMs results in SPR, which yields strong intraband transition [1]. Thus, the above physical process permits the PMNMs to collect the incident light and focus the collected energy near the surface of PMNMs, which in turn transforms the light energy into energy associated with excited charge carriers. The features of PMNMs such as size, shape, and aggregation of nanoparticles as well as the permittivity of surrounding medium decide the intensity of SPR and resonant energy [2]. Several novel surface reactions, namely radiative and non-radiative relaxations, are initiated by the effect of SPR. The influence of SPR leads to the

generation of hot electrons and holes, which are usually termed as hot carriers [3]. These hot carriers can stimulate chemical reactions to the molecules which are present vicinal to the PMNMs [4]. The exceptional characteristics of PMNMs have been extensively employed in numerous applications such as photovoltaic cells, plasmonic sensors, fuel cell fluorescence enhancement as well as local spectroscopies including surface-enhanced Raman spectroscopy (SERS) [5].

Among other analytical techniques, SERS has been deliberated as a commanding analytical technique for the study of surfaces and interfaces. The phenomenon of SERS was initially witnessed in pyridine adsorbed on a rough silver electrode surface in 1974 [6]. Recently, SERS has been utilized as an in situ potential powerful technique that offers unusual surface sensitivity and information regarding molecular fingerprint, to investigate the transient surface species as well as reaction mechanisms. Based on the unique features, SERS has been widely used in medical diagnosis, single molecule detection, pesticide analysis, safety inspections, and identification [7]. Notably, plasmonic metal nanomaterials (such as Ag, Au, and Cu), rough metal films, and gaps between metal surfaces and metal nanomaterials are the widely used SERS platforms for promoting photochemical reactions [8]. The molecules comprising of mostly aromatic or unsaturated bonds are generally targeted for SERS measurements. The Raman signal of the surface species present vicinal to the plasmonic PMNMs can be considerably promoted by the enhanced electromagnetic field, when excited with the appropriate light. Later, the electrochemical SERS had been also employed extensively to investigate the electrochemical processes (interfacial structures, surface reactions, and adsorption of species on electrodes at different potentials) [9]. This measurement has been performed in noble transition nanometals as well as single crystal surfaces for the chemical transformation of aromatic molecules in recent years [10].

From the results of former studies, substituted and unsubstituted aromatic amines as well as nitro compounds have been employed as demonstrative models for aromatic compounds. It is also evident from the earlier studies that an azo species *p,p*-dimer-captoazobenzene (DMAB) can be selectively resulted from the adsorbed substituted or unsubstituted *p*-aminothiophenol (PATP) and *p*-nitrothiophenol (PNTP) on the surface of PMNMs [11]. The PMNMs, pH of the solution, substrate, wavelength, and power of irradiation as well as the environmental conditions can have a strong impact on the above-mentioned conversion [12]. The study of this reaction mechanism is still a challenging issue. The complete thermodynamic and kinetic data are also required for the above system. Therefore, the interpretation of reaction mechanisms, which assist in the optimization of experimental conditions and increasing yield as well as selectivity, can be given by theoretical studies on model reactions.

In this chapter, we have given a brief explanation of SPR and its rapid relaxation of nanometals toward surface hot carriers in Section 2. Then, charge transfer mechanism (metal-to-molecule and molecule-to-metal) and the surface catalytic coupling/condensation of aromatic amines and aromatic nitro compounds on noble metal nanomaterials have been discussed through theoretical and experimental results. Since the experimental conditions are highly dependent on the effect of pH and adsorption of molecule, one of the aromatic amines (PATP) has been taken as a model compound to discuss clearly the effect of pH and adsorption of molecule on the nanometals in Section 3. As DMAB can be selectively resulted from the adsorbed PATP and PNTP on the surface of plasmonic nanostructures during the photochemical reaction, the reported SERS results from chemically synthesized DMAB with experimentally derived DMAB from PATP and PNTP have also been discussed in Section 3. Aerobic oxidation-assisted aromatic amine based on nanoplasmonic photocatalysts will be discussed in Section 4. Finally, the reaction mechanisms and future research prospective have been given Sections 5.

2. Surface plasmon resonance effect on PMNMs and its fast relaxations

The phenomenon of collective excitation of free electrons present in the noble metals when subjected to an external field generates plasmon resonance. For bulk metals, the density of the free electrons decides the characteristic frequency (ω_p) of plasmon resonance, that is, $\omega_p = (4\pi n/m_e)^{1/2}e$; here n = density of conducting electrons, m_e = effective mass, and e = charge unit of electrons [13]. The plasmon resonance frequencies of metals such as gold, silver, and copper in bulk were found to be 9.0, 9.0, and 7.9 eV, respectively. Noticeably, the energy of interband transition is lower compared to the transition energies. This leads to the retardation of intra-band transition, which in turn results in a fairly large damping constant. The fairly accurate relaxation time has been calculated as about 10 fs [14].

Compared to gold, silver, and copper bulk metals, the frequency of SPR gradually shifts to the longer wavelength as the size of metals gets decreased under the surface effect. The lower excitation energy of silver nanostructures hinders the interband pathway, but considerably unusual optical characteristics are displayed by the intraband transition [15]. **Figure 1A** shows the SPR of a spherical PMNMs excited by visible light and the absorption and scattering of light on the noble PMNMs are primarily decided by the effect of SPR. The SPR effect is vital for the formation of sub-wavelength area (hot spot), which results from the conversion of far-field light irradiation into near-field photonic energy [16]. The probing molecules can display the effect of SERS/actuate the reactions of surface photochemistry, as they are adsorbed on the sub-wavelength area. The existence of SPR effect can be observed on transition metals unlike noble metals (copper, gold, and silver). The shorter lifetime of SPR is however due to the following reasons: (i) the radiative relaxation based on the photon emission or (ii) non-radiative relaxation via producing hot carriers. The property of metals, size of nanostructures, energy and the polarization of lasers can also determine the process of relaxation [17].

The size, shape, and dielectric constant of the medium of environment in which the single metal nanoparticles are present determine the frequency of SPR. The SPR lifetime is around 10 fs as the 2.2-eV incident photonic energy falls on gold nanospheres (**Figure 1B**). This results in higher energy photogeneration (around 2.0 eV) of hot electrons compared to the Fermi level, but the energy of the hot hole (lower than the Fermi level) was estimated to be around 1.0 eV [19]. The extinction spectrum of a spherical silver nanoparticle (diameter = 15 nm) shows 380 nm as its SPR frequency. A considerable decrease in the lifetime of hot carriers was observed as the size of silver nanoparticles increased [20]. For instance, in the excitation light, the major distribution of hot carriers was seen surrounding the Fermi level for

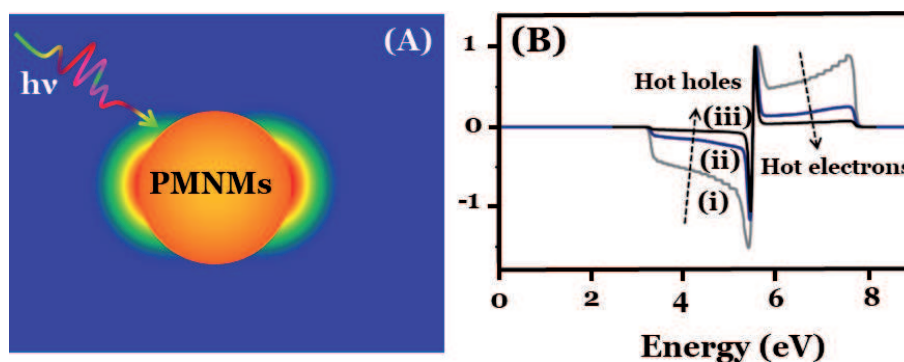


Figure 1. (A) SPR of a spherical PMNMs excited by visible light. (B) Normalized distribution of hot electrons and hot holes on Au slab with thicknesses: (i) 10 nm, (ii) 20 nm, and (iii) 40 nm with incident photonic energy of 2.22 eV (reproduced with permission from Govorov et al., published by Elsevier, 2014 [18]).

the spherical silver nanoparticle possessing a diameter of 25 nm. When the size of metal nanoparticles increases, a considerable increase in the probability of radiation procedure was witnessed unlike nanoparticles with smaller size. In the case of PMNMs, as the lifetime of SPR gets longer, a larger probability in the distribution of hot carriers (high energy) was observed. The lifetime of SPR is longer for spherical silver nanoparticles relative to gold nanoparticles based on the respective interband transition energy values (3.2 and 2.3 eV) [19, 20].

3. Photoinduced charge transfer of aromatic nitro and amino molecules on PMNMs

To illustrate the reaction mechanism, the electroreduction of p-nitrobenzene to aminobenzene derivatives on the surface of noble metals was monitored by SERS. The essential uses of p-substituted aniline as intermediates can be seen in pharmaceuticals and dyes industries. The formation of p-substituted aniline as a result of electrochemical reduction of p-substituted nitrobenzene was revealed from the vanished Raman peak at about 1338 cm^{-1} (corresponding to the symmetric stretching vibration of nitro group in p-substituted nitrobenzene) and appearance of new peaks. Whereas, the mechanistic pathway for the electrochemical polymerization of aminobenzene or aniline was also studied by SERS [21]. Gold colloidal nanoparticles, silver nanofilms, and copper nanoparticles have improved the adsorption and photochemical processes of substituted amino- and nitrobenzenes [22–24]. The reaction mechanisms and the equivalent kinetics are however essential to comprehend the photochemical reactions. All the vibrational frequencies witnessed by our DFT calculations are not highly sensitive to the functional groups such as —OH , —COOH , —SH , —CN , and —NO_2 , which are substituted at para positions of nitrobenzene and aminobenzene. All these substituted aminobenzenes and nitrobenzenes on nanoscale noble metals were chemically transformed to azobenzene derivatives after the photochemical reaction (**Figure 2A**). However, the SERS related to the N=N stretching modes of para-substituted azobenzene exposes an apparently high sensitivity [25]. In addition, the electron density of para functional groups decides the relative intensities of the peaks. The peak appeared at around 1430 cm^{-1} is weaker compared to the peak at around 1390 cm^{-1} in the case of electron-donating functional groups (hydroxyl, amine, and thiol). For electron-withdrawing functional groups (nitro, nitrile, and carboxylic acid), the peak detected at about 1390 cm^{-1} is however weaker than the peak at about 1430 cm^{-1} (**Figure 2B**).

We have given the possible photochemical reaction mechanism for the reduction and oxidation of substituted aromatic nitro and amino compounds into corresponding azobenzene derivatives (**Figure 3A and B**). The substituted amino molecules transformation into azobenzene derivatives in the presence of light involves two steps: 1. Oxidation of amino molecules, and 2. Coupling of two oxidized amino molecules into disubstituted azobenzenes, whereas, the reduction of amino-substituted nitro molecules transformation into azobenzenes in the presence of light involves three steps: 1. Reduction of nitro molecules, 2. Condensation of reduced nitromolecules to oxadia-ziridine, 2,3-bis (4-mercaptophenyl), and 3. Further oxidation of Oxadia-ziridine can convert 2,3-bis (4-substituted phenyl) into disubstituted azobenzene. The experimental results from the oxidation/reduction of different para-substituted aminobenzene/nitrobenzene into para-substituted azobenzenes nevertheless depends on the experimental conditions along with the laser powers

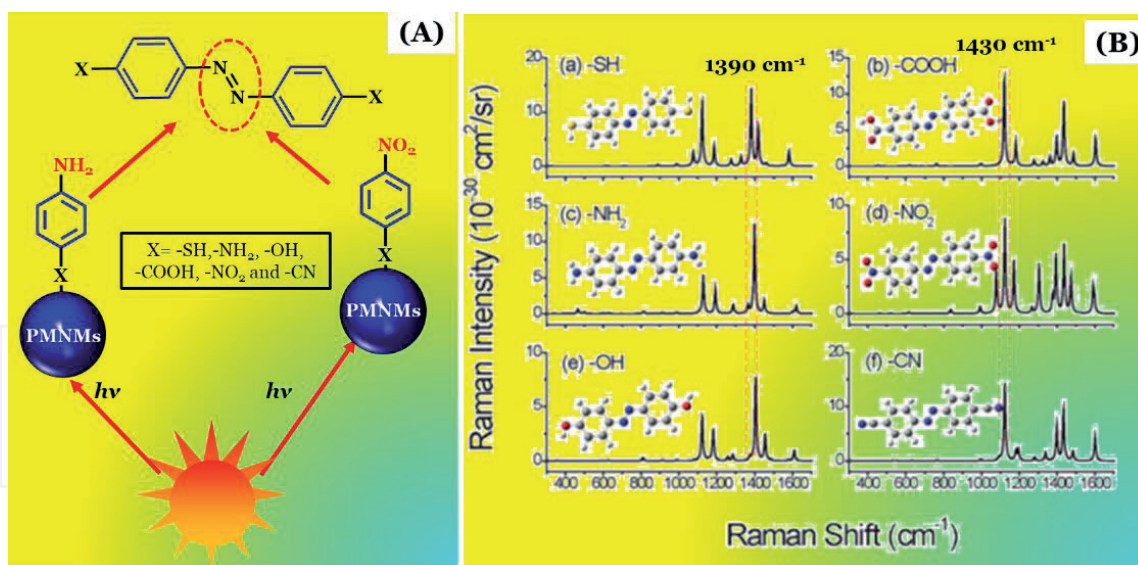


Figure 2. (A) Schematic representation for photochemical transformation of substituted amino and nitrobenzenes to azobenzene derivatives. (B) Raman spectra of azobenzene derivatives with various para functional groups simulated by PW91PW91/6-311 + G(d, p): (a) -SH, (b) -COOH, (c) -NH₂, (d) -NO₂, (e) -OH, and (f) -CN. (reproduced with permission from Zhao et al., published by RSC, 2012 [25]).

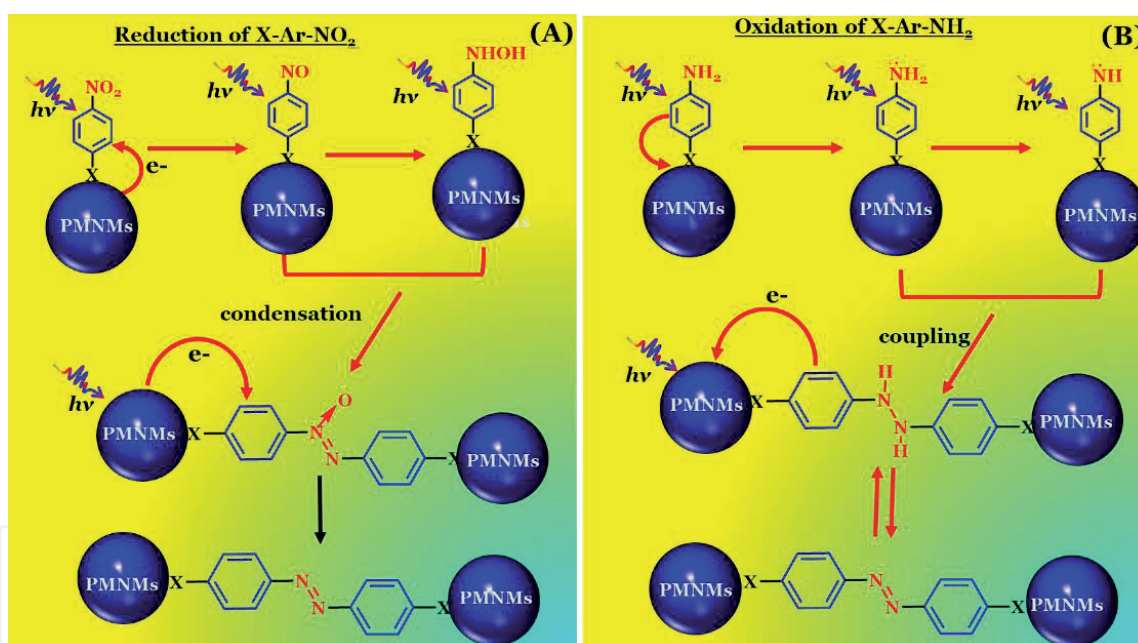


Figure 3. Schematic representation of reaction mechanism for the photochemical reduction of X-ArNO₂ (A) and oxidation of X-ArNH₂ (B) (X = -OH, -COOH, -SH, -CN, and -NO₂).

employed for Raman excitation, electrolyte pH as well as adsorption that promotes the electroreduction of nitro groups into aromatic amines or azo compounds. Thus, numerous studies have been developed for studying the surface reactions of the above mentioned SERS molecules.

Among other substituted aromatic nitro compounds, SERS has been employed widely to study the photochemical as well as electrochemical reduction of p-nitrobenzoic acid (PNBA) and p-nitro-thiophenol (PNTTP) [26]. The decrease in the intensities of several original peaks and appearance of several new peaks take place in the course of cathode polarization/laser irradiation. Nonetheless, the detailed study for the above spectral alterations is still contentious. The appeared new peaks

are in concordance with the observed SERS results of aromatic amines adsorbed on silver nanostructures [27]. Thus, some studies equate the new peaks to aromatic amines as reduction products. For example, Sun et al. described that, the product formed can be both aniline species and azo compound or individual aniline species/ azo compound. They proposed the charge transfer mechanism where the transfer of charge between silver island films and p-nitrobenzoic acid arose from the laser excitation [28]. The high-power laser irradiation also resulted in the formation of p, p-azodibenzoic acid through reductive coupling reaction [29].

p-aminothiophenol (PATP) is a molecule possessing thiol group at the para position of aniline. It can form self-assembled monolayer (SAM) on the surface of nanometals. Additionally, PATP has been targeted as a significant surface probe molecule in the areas of SERS and nanoscience. An exceptional and sturdy SERS signal has been displayed by PATP. However, the study of enhancement mechanism is still challenging since/in 1990s. An intense potential-dependent peak of SERS for three excitation wavelengths (488, 514.5, and 633 nm) was seen at 1430 cm^{-1} [30]. As the excitation wavelength increases, the potential analogous to the maximum Raman peak intensity proceeds toward the direction of more negative potential [30]. This reveals that these light irradiations can perform the charge transfer from the PMNMs to adsorbed surface species. From DFT calculations of metallic cluster models, we have proposed a clear theoretical pathway for the charge transfer mechanism from PATP to PMNMs and PMNMs to PNTP in (Figure 4). In the course of incident light excitation on the surface of rough/colloidal silver and gold, the participation of surface plasmon and charge transfer processes have been described. At this juncture, for oxidation and reduction reactions, the metal nanoparticles act as sink of electrons and electron source. The Fermi level of PMNMs which exists in between HOMO and LUMO of PNTP or PATP (adsorbate) can be altered by the applied potential. The resonant charge transfer can occur as the energy difference between the ground state ψ_g and the photon-driven charge transfer excited state ψ_{CT} equates the exciting radiation energy. Thus, the charge transfer takes place from the molecule to the

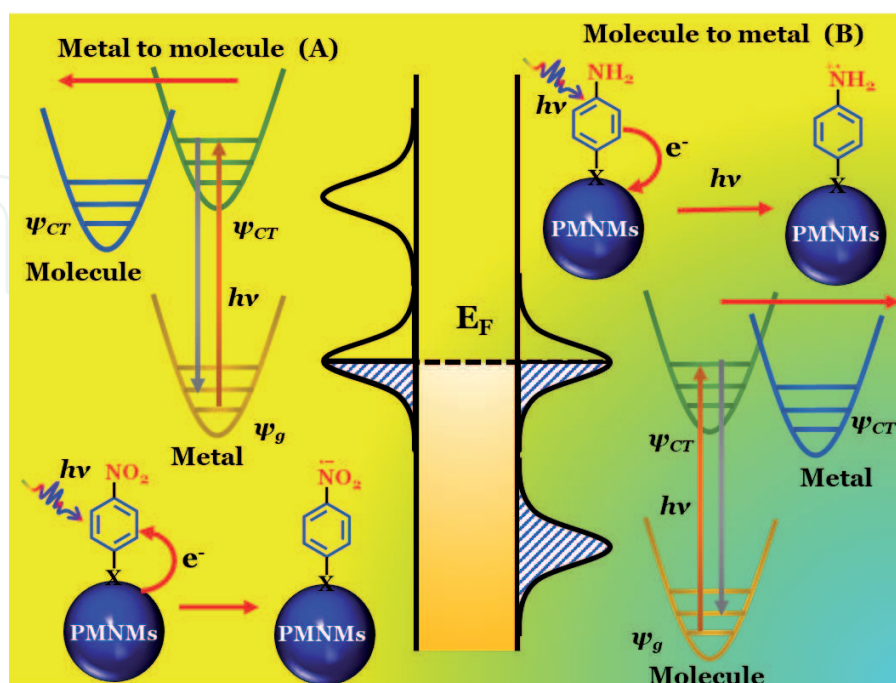


Figure 4. (A) Schematic representation of charge transfer from metal to molecule: an electron excitation from the Fermi level of PMNMs to the LUMO of aromatic nitro compounds. (B) Charge transfer from molecule to metal: an electron excitation from the HOMO of aromatic amine to the Fermi level of PMNMs.

surface of silver for X–ArNH₂ and from silver surface to molecule for X–ArNO₂. In both cases, X symbolizes the thiol functional group at the para position. Later, the excited surface complex possibly will go through one of the two dissimilar deexcitations as follows: (i) based on the reverse charge transfer back to ground state which is followed by a radiative process, where, this deexcitation (purely physical) comprises of either Raman scattering or fluorescence emission and (ii) photochemical reaction. Here, a neutral ArNO₂H radical can be formed by the excited nitro radical anion, which takes up proton from proton donors present in solution. Further reactions take place from the so formed neutral ArNO₂H radical. The neutral ArNH radical formed from the excited amine radical cation by giving out a proton. This ArNH radical can undergo nitrogen-nitrogen coupling reaction (dimerization), indicating the molecules are strongly adsorbed on the electrode surface (**Figure 2**). Thus, the charge transfers from molecule (PATP) to metal nanoparticles and metal nanoparticles to molecule (PNTP) occur. In fact, the experimentally observed charge transfer should be responsible to a process from silver electrode to adsorbed DMAB species, as proposed from previous DFT calculations [25].

3.1 Effect of pH toward photochemical reaction on PATP-adsorbed PMNMs

In order to give a clear explanation of the effect of pH, adsorption of molecules for surface catalytic coupling reactions, and oxygen-assisted photocatalytic reactions on PMNMs, we have chosen only para-aminothiophenols (PATPs) as representative compounds. The SERS signals are highly sensitive to the pH of the electrolyte and applied potential. It is evident from the previous SERS measurements of the adsorption of PATP on the surface of rough silver and gold electrodes, reported by Hill and Wehling [31]. The property of SERS significantly varies from acidic to alkaline medium. For the case of anodic and cathodic polarization, SERS spectra of PATP show substantial variations in alkaline solution. In contrast to alkaline medium, a good reversibility behavior (in intensity of SERS) was seen in acidic medium based on changing potentials. As the applied potentials move toward the negative direction, the SERS peaks (1130, 1390, and 1440 cm⁻¹) retained virtually in the alkaline medium. In order to describe the above character, an isomerization of aromatic and quinonoidic configurations was postulated for PATP adsorbed on the surface of metal electrodes in acidic medium. Under negative applied potential (–1.4 V vs. Ag|AgCl) in pure sodium disulfide, the quinonoidic configuration was proposed in alkaline medium to support the above hypothesis. Based on the adsorption of PATP in the nanoscale cavity between the substrate (gold) and silver nanoparticles, the isomerization and charge transfer mechanism are given concurrently to the SERS mechanism by Zhou et al. [32]. Till now, we know these changes of SERS are closely associated with the surface catalytic coupling reaction of PATP to DMAB.

3.2 Adsorption configurations of PATP on PMNMs

The three adsorption features feasible as PATP toward the surface of metal are: (i) formation of strong chemical bonds (Au—S or Ag—S bond) when the easy binding of thiol group with gold/silver takes place, (ii) simultaneous breaking of S—H bond, and (iii) the formation of weak coordination bonds (Au—N or Ag—N bond) as the amino group moves closer to the surface of metal [33]. As a result, there is concurrent binding between the surface of metal and thiol as well as amino groups. On the metal surface, the top, bridge, and hollow sites possessing large adsorption energies can hold the sulfur atoms (**Figure 5A**). The adsorption configuration exposing a skewed angle with regard to the surface has been observed as the top/bridge sites hold the thiol group. In the case of hollow sites, the molecular

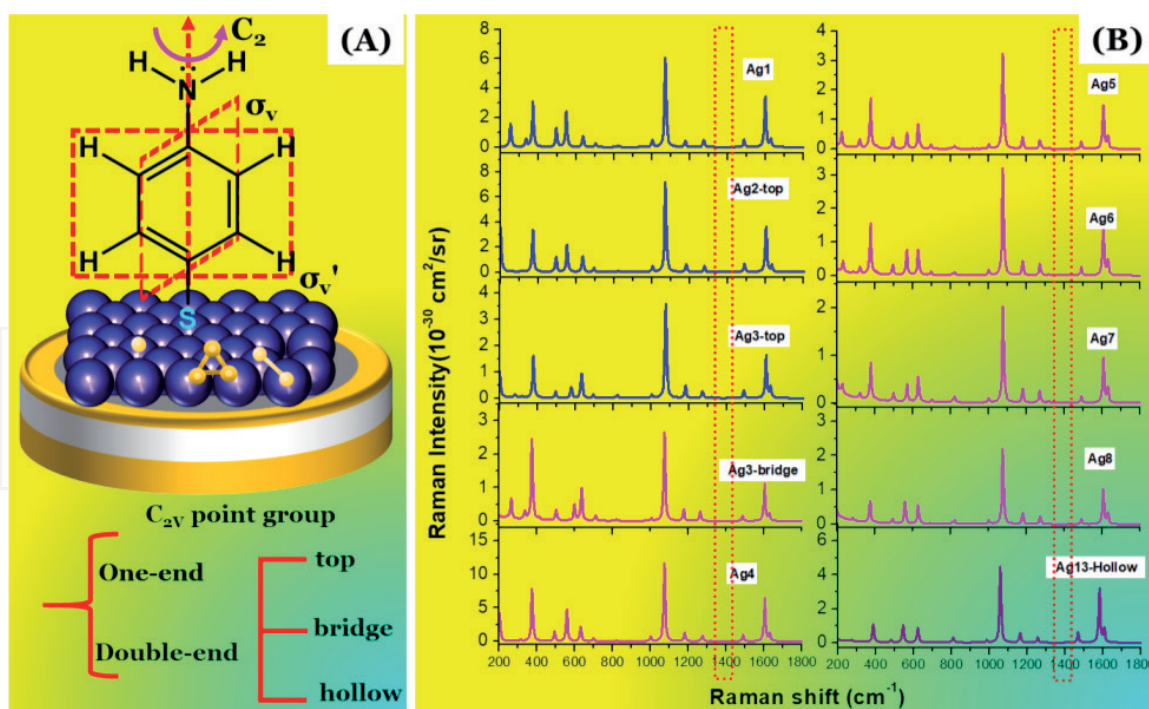


Figure 5. (A) One-end adsorption configuration at a top site, a bridge site, a hollow site, and double end configuration through the interaction between C_{2v} point group of amino nitrogen binding and silver. (B) Simulated Raman spectra of PATP with different silver clusters using DFT theoretical methods ($B_3LYP/6-311 + G^{**}(C, N, S, \text{ and } H)/LANL2DZ(Ag)$) (reproduced with permission from Wu et al., published by ACS, 2009 [33]).

symmetric axis of PATP can be visualized as perpendicular with respect to the surface. A skewed angle (about 60°) was observed with regard to the line normal to the surface.

The adsorption configurations of PATP on PMNMs can be easily understood from our DFT calculations [33]. The simulated Raman spectra of PATP adsorbed on various silver clusters have been shown in **Figure 5B**. The frequencies of intense peaks observed at $379, 630, 1001, 1071, 1167, 1336, 1476,$ and 1596 cm^{-1} can be related with the peak frequencies at $379, 630, 1010, 1080, 1181, 1334, 1489,$ and 1588 cm^{-1} . Here, the latter peak frequency values represent the PATP adsorbed (in aqueous acidic solution) on a rough silver electrode [31]. The strongest Raman peaks appear at 1071 and 1596 cm^{-1} . These peaks symbolize the absolutely symmetric mixed vibrational modes of C—C and C—S stretching and the C—C bonds stretching parallel to C_2 axis when we assume PATP with a symmetric point group of C_{2v} . Here we assumed that the backbone of the adsorbed PATP has a local and approximate C_{2v} symmetry of point group, as shown in **Figure 4A**. The totally symmetric in-plane bending vibration of C—H bonds can be observed at 1181 as well as 1489 cm^{-1} . In the case of free as well as adsorption states, PATP has been anticipated to be in C_{2v} point group. The four vibrational modes ($1125, 1286, 1322,$ and 1426 cm^{-1}) with low Raman intensity present in between 1100 and 1450 cm^{-1} possess b_2 symmetry, which correspond to the asymmetric stretching of C—C bonds and in-plane bending vibrations of C—H bonds. Our results along with the study of vibrational analysis of free and adsorbed PATP revealed the deficit vibrational fundamental frequencies at about 1390 cm^{-1} . This shows the significant dissimilarity between experimental as well as theoretical Raman spectra [30, 31]. In spite of the photon-driven charge transfer Herzberg-Teller vibronic coupling, a likely intense peak of SERS cannot be offered by the chemical enhancement mechanism of PATP. The spectra of PATP adsorbed on silver, gold, as well as copper were investigated in various configurations in order to comprehend the vibronic coupling

enhancement in the SERS spectra of PATP. These conclusions lead to the initial hesitation for the strong SERS peaks only related to the earlier elucidated photo-driven charge transfer enhancement mechanism of adsorbed PATP.

In analysis of low-lying excited states, a photo-driven charge transfer reaction takes place from PATP toward the surface of metal. This has been also revealed from our density functional theory (DFT) studies [34]. Additionally, the energies of low-lying excited states have been evaluated by using a molecule-metal cluster modeling system. The charge transfer energies for PATP-to-silver clusters (~ 2.28 eV) and PATP-to-gold clusters (~ 2.08 eV) were estimated in the case of PATP- M_n clusters, where $n = 13$. The energies of transition from M_n clusters to PATP for charge transfer excited states were additionally examined to be higher than 3.0 eV [35]. This reveals that in common SERS measurements, the incident photonic energies are lower when compared to the charge transfer energies from metal toward PATP. Furthermore, it has been found that the interband transition energies of gold are lower than the energies of charge transfer and the interband transition energies of silver are nearer to the energies of charge transfer. Thus, under the irradiation of visible light, the photon-driven charge transfer should take place from PATP towards metal surfaces. This direction of charge transfer has been revealed from our early DFT calculations. When the wavelength of laser increases, the maximum potential in the potential-dependent SERS intensity profile should travel toward the positive direction. Our theoretical results were in concordance with the results of theoretical studies from other groups [36, 37]. In contrast, our results were incoherent with the earlier proposed SERS results of PATP adsorbed on surfaces of various metals [30]. This above deviation deliberates the additional uncertainty on the SERS signal appeared.

3.3 Surface catalytic coupling reactions on PMNMs

We observed that the mentioned charge transfer mechanism cannot be suitable for all the experimental studies. Here, two main key contradictions were observed as follows: (i) SERS peaks at 1140, 1390, and 1426 cm^{-1} appeared in Raman excitation wavelengths from 488 to 1064 nm for PATP-adsorbed silver and gold surfaces [32, 38]. The same SERS peaks were also acquired in the nanocavity between silver nanoparticle and smooth gold substrate that employs the wavelength of 1064 nm [32]. The UV-Visible absorption peak at 295 nm ($\pi \rightarrow \pi^*$ transition) of PATP in methanol solution resembles transition energy of about 4.20 eV, whereas, SERS peaks arising from photo-driven charge transfer are in the range of 1.16–2.54 eV (corresponding to the incident photonic energy), which would contradict the predicted charge transfer transition. Therefore, if the charge transfer enhancement mechanism was categorized as a resonance-like Raman scattering process, this is the inconsistent large energy gap between the intramolecular excited state and the charge transfer excited state [39–41]. (ii) Another important contradiction is the pH effect. In acidic solutions, the reversible behavior of intensity ratios of SERS peaks (from 1440 and 1080 cm^{-1}) was described with respect to the potentials applied in the earlier studies. Some studies used isomerization to elucidate the reversibility nature with applied potentials. In the case of alkaline solutions, the elucidation of irreversible behavior is not possible. In addition, the correlation between the reversible and irreversible nature in both acidic as well as basic solutions was not simply explained on the basis of charge transfer mechanism.

Motivated by the experimental results, the probable surface species have been reassessed. We have proposed three different surface species for adsorption of PATP on the surface of PMNMs (**Figure 6A**). (i) PATP was oxidized to 4'-mercapto-4-aminodiphenylamine by increasing the potential anodically at PATP-adsorbed gold and platinum metal surfaces. Conversely, a quite different simulated Raman

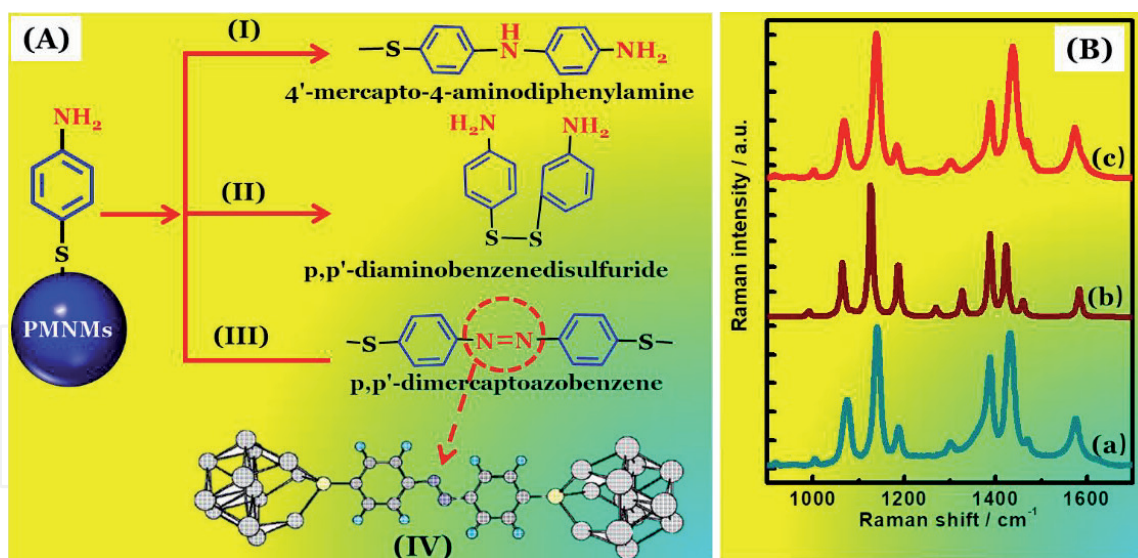


Figure 6.

(A) The three possible reaction pathways of PATP adsorbed on nanostructured metal surfaces after the photochemical reactions (I), (II), and (III). A theoretical adsorption configuration of DMAB adsorbed on rough metal surfaces (IV). (B) SERS spectrum of synthesized DMAB (a), simulated Raman spectrum of DMAB on two silver clusters using DFT (PW91PW91/6-311 + G^{**}(C, N, S, and H)/LANL2DZ(Ag) level (b)), and SERS spectrum from PATP adsorbed on silver nanoparticles measured with the excitation at 632.8 nm (c).

spectrum was observed for the PATP adsorbed on silver electrodes [30]. (ii) The formation of *p,p'*-diaminobenzenedisulfuride was observed for PATP adsorbed on silver films, wherein the disulfide compound was believed to form from its corresponding azo compound [42]. However, the disulfide bond will be shattered because of the strong Ag-S bond on silver surfaces [43]. (iii) Chemical transformation of PATP to DMAB (*p,p'*-dimercaptoazobenzene) was due to the surface catalytic coupling reaction on noble metal surfaces. We suggested that PATP adsorbed on noble metal surfaces can transform to DMAB under irradiation of visible laser based on our DFT and experimental results [33, 44].

DMAB complex was calculated on the basis of static polarizability derivatives. Moreover, DMAB complex and DMAB-Ag_n complexes were also obtained by a single-end configuration, but the observed Raman spectra were found to be very similar [33, 34]. In particular, the vibrations of azo (N=N) and benzene ring result in the strong Raman peaks. The theoretical and experimental results from Sun and Xu support the above interpretations [45, 46]. Considerable influence of Ag—S vibrational frequencies was also observed by the corresponding strong Raman peaks because of the localization interaction of sulfur and silver clusters. Furthermore, the active Raman modes (A_g and B_g) are the irreducible representations for symmetric center trans DMAB to C_{2h}. The strong Raman peaks at 1130, 1390, and 1440 cm⁻¹ thus mainly appeared from azo group and benzene ring symmetric vibrations of DMAB [(44)]. The peak at 1130 cm⁻¹ resembles C—N symmetric stretching vibration and the peaks at 1390 and 1440 cm⁻¹ show the mixed vibrations of the N=N bond stretching and the C—H in-plane symmetric bending [33, 44]. By our DFT calculations, we concluded that proper functional is very important to predict the N=N bond distance, since the positions of latter two strong peaks are crucial. Theoretical frequencies were in good agreement with the experimental frequencies when the PW91PW91 functional was combined with the triple-zeta Gaussian basis set 6-311 + G^{**}, whereas, the theoretically and experimentally observed vibrational frequencies are pointedly overestimated when B3LYP functional was used. Two different N=N bond distances for DMAB were calculated to be 1.273 Å (by PW91PW91/6-311 + G^{**}) and 1.256 Å (by B3LYP/6-311 + G^{**}) [33]. Other reports

by gas electron diffraction showed comparable result with the experimental value (1.260(8) Å) of azobenzene [47, 48]. **Figure 6B** shows the theoretically simulated Raman spectrum of DMAB (b) is in a good agreement with experimental spectra of DMAB interacted with two silver clusters (a). But for DMAB, such a Raman spectrum for PATP adsorbed on silver cannot be obtained even under the consideration of the photon-driven charge transfer mechanism. Duan and Luo reported that experimentally observed SERS peaks of DMAB adsorbed on silver surfaces are the same as the theoretically observed SERS peaks for DMAB adsorbed on silver surfaces [49]. This was considered due to the tension effect of the adsorption on silver surfaces.

The intramolecular resonance effect can be contributed to DMAB adsorbed metallic nanostructures since DMAB is a dye molecule, which owns its absorption band in the visible region. We also observed that charge transfer takes place from silver to DMAB molecule in the low-lying excited states. Recently, we reported the resonance-like enhancement effect of photo driven charge transfer mechanism and intramolecular electronic transition [33, 34]. As the molecular orbitals are mainly distributed in the DMAB azo group ($>C=N=N-C<$), azo Raman peaks at 1130, 1390, and 1440 cm^{-1} strongly match with the photonic energies to the intramolecular resonance energy, relative to other Raman peaks at 1078 and 1596 cm^{-1} . Because of surface plasmon resonance and intramolecular resonance effects, SERS peak of DMAB appeared very easily after the oxidation of PATP through the surface catalytic coupling reaction. Based on the deep studies, the SERS spectrum of DMAB follows the surface-enhanced resonance Raman spectroscopy in the visible region. This study also revealed that the enormous enhancement effect can be observed in the SERS spectrum of PATP adsorbed on silver or gold nanostructures. The key factors such as acidity and applied potentials influence the stability of DMAB at electrochemical interfaces [50]. Therefore, DMAB can be converted into PATP in acidic solution, due to the reversibility of applied potentials in acidic solution [51]. Even though, DMAB is more stable in the alkaline solution, it can be reduced into PATP at more cathodic or negative potentials.

The charge transfer mechanism was also engaged to study the Raman spectra of DMAB at silver/gold surfaces and PATP on silver or gold substrates. In the case of DMAB, the photon-driven charge transfer is from metal (silver or gold) to DMAB, whereas, photo-driven charge transfer occurs from PATP to metals under visible light for PATP adsorbed on silver or gold substrates. Therefore, charge transfer directions are opposite for low-lying excited states of PATP and DMAB. Moreover, the reversibility or irreversibility of DMAB is strongly dependent on acidity of aqueous solutions.

Kim and coworkers studied the abnormal SERS peaks arising from the view of CT mechanism in various conditions such as pH, rotation, temperature, and reducing agent as follows [52]. They observed SERS peaks at 1130, 1390, and 1430 cm^{-1} in an acidic solution with $\text{pH} = 3$. SERS signals of the —NO_2 symmetric stretching gradually disappeared when PNTP was adsorbed on a rotation platform with 3000 circles per minute modified with silver nanoparticles. They visualized the strong peaks at 1130, 1390, and 1430 cm^{-1} after 30 min. It was believed that the strong peaks appeared only from the PATP, and not from PNTP. They concluded that no photochemical reaction occurred for PATP at the boundary of ice and silver nanoparticles at liquid nitrogen temperature (77 K) on the basis of nonexistence of reaction for PNTP at the same boundary [52]. Even when strong reductants such as NaBH_4 exist, they still observed abnormally strong SERS peaks. It may be assumed that such a significant SERS band should be observed only in the SERS spectra of PATP and DMAB adsorbed on noble metals.

The reaction mechanisms and their dynamics of PATP and PNTP are very different. The activation energy of the rate determination steps for PATP and PNTP on

silver surfaces was calculated to be 5 and 12 kcal/mol, respectively. It indicates that the PATP oxidation reaction rate is quite fast so that an early photochemical reaction cannot be identified. The lack of thermodynamic properties and kinetic information for these reactions are observed in certain studies, which deal with the reaction mechanisms. Our opinions regarding the above issue as well as the anticipated reaction mechanisms will be discussed in the next section.

4. Aerobic oxidation-assisted aromatic amine on PMNMs photocatalysts

The mechanism for the electrochemical reduction of aromatic nitro compounds into aromatic amines at electrode interface has been reported by Haber in 1898 [53]. The catalytic oxidation of aniline to azobenzene on TiO₂-reinforced gold nanoparticles (in the presence of oxygen atmosphere) was proposed by Grirrane et al. [54]. After that, several oxidation and reduction reactions of aminobenzene and nitrobenzene have been reported to form azobenzene. However, limited number of mechanisms (which strongly depend on experimental conditions) have been investigated as silver/gold nanomaterials based on photochemical and photoelectrochemical processes under visible light [55]. The respective absorption bands for PATP and PNTP occur around 300 and 326 nm revealing the absence of absorption peaks of the above two molecules in visible light region [30]. Interestingly, many studies reported that the surface reactions of PATP and PNTP chemically transformed into DMAB in the presence of visible light regions using SERS. Therefore, the adsorbed and photochemical reacted PATP and PNTP molecules on PMNMs needed for the new pathways under SERS investigation.

The activation of O₂ is found to be one of the most significant steps in the case of catalytic oxidation reactions. The activation of O₂ into two weakly-bonding oxygen atoms has been achieved by employing silver anions and gold clusters [56]. The binding nature of negative metal clusters with oxygen is stronger, compared to neutral metal clusters. The surface plasmon-mediated injection of an excited electron from the optically excited silver nanoparticles toward adsorbate can activate O₂ into two weakly-bonding oxygen atoms as reported by Christopher et al. [17, 57]. Oxygen adsorption on the surface of plasmonic nanostructures may involve direct as well as indirect charge transfer reactions. On the other hand, no clear evidences are available to describe that either the direct or indirect charge transfer reactions played the significant part [58]. The study of activation mechanism of oxygen is the challenging part, because of the catalytic oxidation reaction taking place on the surface of plasmonic metal nanoparticles, which involves the direct participation of O₂ in metal-oxygen battery systems.

The renowned surface plasmon resonance has been displayed in **Figure 7A**. After the optical excitation of surface plasmon, there are two probable channels of relaxation. The process of scattering (radiative decay into photons) or absorption (non-radiative decay into electron-hole pairs) may result in surface plasmon damping (**Figure 7B**). When the volume of nanoparticle increases, the ratio of scattering to absorption gets increased on the basis of discrete dipole approximation (DDA) simulation and Mie theory calculation [59]. Aimed at the nanoparticles in very small size, the generation of electron-hole pair acts as the foremost pathway to decay. In order to demonstrate the dynamics of excited electrons and holes as well as energy levels, several theoretical models were developed. Based on first-principle TD-DFT calculations [60], we have recently studied the photoinduced excitation of small metal clusters. The evaluated TD-DFT results are in concordance with the distribution results of plasmonic carriers in gold and silver nanoparticles, which were acquired from the quantum equation of motion for the density matrix (18). Because

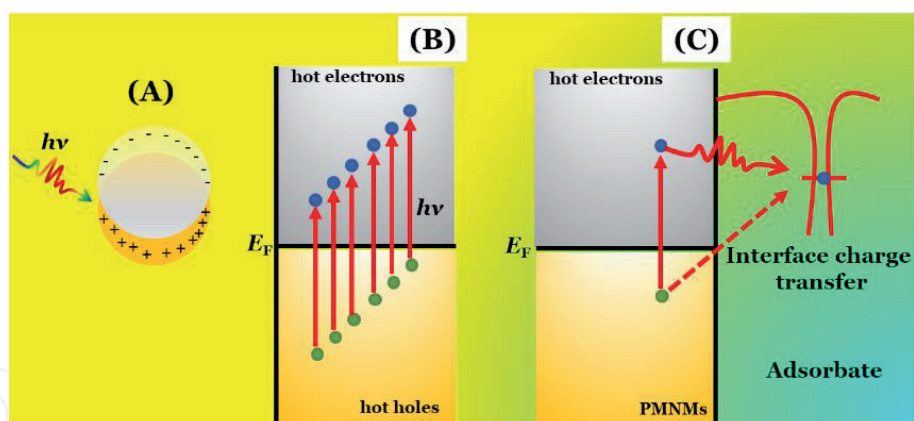


Figure 7. (A) Schematic representation of coherent optical excitation of SPR on noble metal surfaces. (B) Hot electron-hole pairs created by non-radiative decay of SPR. (C) Surface plasmon-induced hot electron injection to adsorbed oxygen molecules.

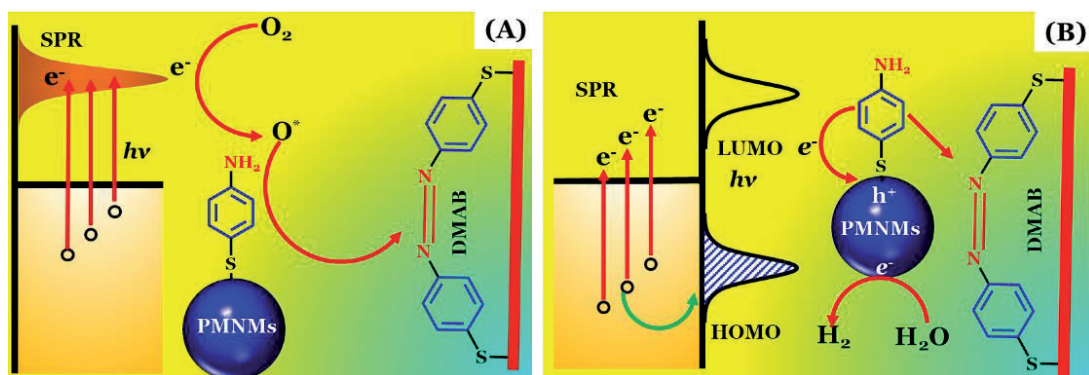


Figure 8. (A) Schematic representation of surface oxidation coupling reaction for PATP-adsorbed PMNMs by surface oxygen species activated by hot electrons under the excitation by visible light. (B) The hot-hole oxidation mechanism for PATP adsorbed PMNMs in the solid/liquid interfaces.

of their higher energy, hot electrons will extend further away from the nanoparticle surface than an equilibrium electron distributed at the Fermi level. As shown in **Figure 7C**, the electron acceptor (oxygen adsorbed on a nanoparticle surface) located nearer can accept the hot electron tunneling to its unoccupied orbitals. This effective reaction is equivalent to the process occurring in the metal-semiconductor composites [20].

The broader absorption bands observed in the region of visible light are due to the influence of sturdy surface plasmon resonance. The generation of hot electron-hole pairs by the process of irradiation relaxation depends on the lifetime (10–20 fs) of localized SPR. The oxygen molecules can be reduced into active oxygen species (under oxygen atmosphere) by the hot electrons (reducing nature) produced at the surface of metal. Thus, adsorbed PATP on silver nanoparticles can be oxidized by the active oxygen atoms (**Figure 8A**). Here, the oxidation of amine group results in the formation of respective imine/free radical. Later, hydroazobenzene was formed due to dimerization. Further oxidation leads to the formation of adsorbed DMAB on the surface of silver nanoparticles [60].

In the absence of active oxygen species, the hot-hole oxidation mechanism for the conversion of PATP into DMAB has been displayed in **Figure 8B**. The presence of interfacial defects/small clusters lengthens the lifetimes of hot electrons or holes on the surface of PMNMs. The energy of the hot hole at interfaces and the energy position of the occupied orbital were alike for the adsorption of PATP on the surface of metals [25, 60]. Thus, PATP can form a cation free radical upon oxidation. The

intermediate formed can give out a proton to neutral imine free radical in alkaline/neutral solution. This can be further dimerized and oxidized for the formation of DMAB, parallel to the oxidization reaction based on surface-active oxygen species [61]. Because of the SPR effect, a larger value of rate constant has been exposed by the hot-hole oxidization mechanism unlike the direct charge transfer process.

The experimental environments decide the hot-hole oxidation mechanism for the adsorption of PATP on the surfaces of noble PMNMs. Various investigations have been reported for the generation of electron-hole pairs, which prompts the chemical reactions on the surface of semiconductors. Once the electron-hole pairs got separated, the electrons (present in conduction band) involve in the process of reduction and the holes (present in valence band) are responsible for initiating oxidation. An apparent decrease in the lifetimes of hot electrons and holes was observed as the persistent distribution of energy band seen around the Fermi level on the PMNMs [62]. On the surface of noble PMNMs, the lifetime of hole is frequently found to be in femtoseconds [63]. The lifetime of excitation electrons (associated with its excitation energy) in the excited sp-band is lower than the lifetime of d-band holes [64]. The involvement of hole in the chemical processes has been deliberated in limited reports. The relationship of excitation wavelengths with the pH values has been presented by our results. The conversion of PATP into DMAB based on the oxidation coupling reaction is a multistep reaction comprising of electron/hole transfer as well as proton transfer steps. The values of applied potential, pH of solution, and incident photonic energy decide the chemical potentials of hot electrons, holes as well as protons in the electrochemical SERS measurements [60]. As the incident photonic energy increases, an increase in energies of hot electrons and holes was observed. In contrast, a decrease in their lifetimes with regard to the Fermi level was observed. When the pH value of the solution increased, a decrease in the chemical potential of protons present in the interfacial solution phase was observed. The increase in the energy of hot-hole pairs as well as the value of pH supports the oxidation of PATP into DMAB with loss of two electrons and two protons for each surface reactant. This is complicated but interesting.

5. Summary and prospects

As the molecules from liquid/gas phase proceed toward the surface of metal, considerable variations in the optical physical and chemical characteristics are observed. SERS as well as surface photocatalytic chemical reactions explain the above characteristic variations on PMNMs. Herein, the oxidation and reduction reactions of PATP and PNTP on the surface of PMNMs were described. In addition, the reaction mechanisms based on these aromatic compounds were investigated in the region of visible light, where the surface plasmon resonance appears on nanostructures of noble metals. The photo-driven charge transfer and the interfacial chemical reactions take place because of the hot electrons and holes generated from SPR relaxation. The hot electrons actuate the surface-activated oxygen species, which result in the surface catalytic coupling reaction in gas/solid interfaces. Relative to the activation barrier of gold nanostructures, the activation barrier of silver nanostructures is smaller. It is evident from the DFT calculations in simulated SERS and chemical reaction pathways. These calculations and SERS measurements describe the reason for the occurrence of highly selective and rapid oxidation coupling reaction of PATP. Relative to photooxidation of PATP on PMNMs, the photoreduction of PNTP is apparently slower. A steady decrease in the SERS signal of the symmetric stretching vibration (nitro group) was observed in the photoreduction reaction. The emphatic evidences for the photooxidation of adsorbed PATP

on metal nanomaterials is inadequate compared to the evidences for the conversion of PNTP to DMAB. The main reason is the former reaction is much faster than the latter one. The primary outcomes for the photoreduction and photooxidation processes have been given through theoretical as well as experimental investigations. In addition, the effect of pH, power of laser, incident wavelengths, and oxygen assisted on photoreduction/photooxidation were tried to be made clear.

The study of the effect of enhancement mechanism resulting from surface plasmon resonance on the thermodynamic and dynamics of chemical reactions of metals in nanoscale dimensions is an interesting area. The SPR can enhance the local surface optical electric field on the surface of PMNMs, which in turn increases the charge transfer probability between metal and molecules. The chemical reactions on the surface were actuated by the hot electrons and holes generated from the SPR relaxation. The processes result in surface transient active species inclusive of anions with negative charge and free radicals carrying positive charge. However, there is lack of evidence available for the initial reaction steps taking place on the surface of PMNMs.

The major concern for hot electrons can be observed only in the photochemical reactions on the surface of PMNMs. A contemporary consideration of hot electrons as well as the hot holes is essential for a complete system of chemical reaction. For the transformation of light energy in-to chemical energy, a stable and reliable system can be created by PMNMs. The hot holes were attracted to the surface of PMNMs after the completion of PATP photooxidation. But, the retention of hot electrons reduces the surface oxidation species as well as hydrated protons and water molecules into hydrogen gas. The hot electrons present on the surface of PMNMs moreover result in hydrated electrons, which reduces the oxygen species in solution phase. Here, the oxidation reactions are actuated by the hoarded hot holes on the surface of PMNMs. In addition, water molecules in aqueous solution can be oxidized into oxygen gas in the presence of hot holes. On the basis of SPR effect, these photochemical surface reactions actuate chemical processes for the transformation of light energy to chemical energy. The above mentioned surface plasmon-mediated chemical reactions, can find promising applications in the enhancement of light energy efficiency in photocatalytic fuel cells and dye-sensitized and new perovskite solar cells.

Acknowledgements

This work was financially supported by the National Science Foundation of China (21533006 and 21373172).

Conflict of interest

The authors declare no conflict of interest.

IntechOpen


IntechOpen

Author details

Rajkumar Devasenathipathy, De-Yin Wu* and Zhong-Qun Tian
State Key Laboratory of Physical Chemistry of Solid Surfaces, Department of
Chemistry, College of Chemistry and Chemical Engineering, Xiamen University,
Xiamen, China

*Address all correspondence to: dywu@xmu.edu.cn

IntechOpen

© 2019 The Author(s). Licensee IntechOpen. This chapter is distributed under the terms of the Creative Commons Attribution License (<http://creativecommons.org/licenses/by/3.0>), which permits unrestricted use, distribution, and reproduction in any medium, provided the original work is properly cited. 

References

- [1] Schuller JA, Barnard ES, Cai W, Jun YC, White JS, Brongersma ML. Plasmonics for extreme light concentration and manipulation. *Nature Materials*. 2010;**9**(3):193
- [2] Hartland GV. Optical studies of dynamics in noble metal nanostructures. *Chemical Reviews*. 2011;**111**(6):3858-3887
- [3] Zhan C, Wang Z-Y, Zhang X-G, Chen X-J, Huang Y-F, Hu S, et al. Interfacial construction of plasmonic nanostructures for the utilization of the plasmon-excited electrons and holes. *Journal of the American Chemical Society*. 2019;**141**(20):8053-8057
- [4] Zhao L-B, Liu X-X, Zhang M, Liu Z-F, Wu D-Y, Tian Z-Q. Surface plasmon catalytic aerobic oxidation of aromatic amines in metal/molecule/metal junctions. *The Journal of Physical Chemistry C*. 2016;**120**(2):944-955
- [5] Yu H, Peng Y, Yang Y, Li Z-Y. Plasmon-enhanced light-matter interactions and applications. *npj Computational Materials*. 2019;**5**(1):45
- [6] Fleischmann M, Hendra PJ, McQuillan AJ. Raman spectra of pyridine adsorbed at a silver electrode. *Chemical Physics Letters*. 1974;**26**(2):163-166
- [7] Liu Y, Yang D, Zhao Y, Yang Y, Wu S, Wang J, et al. Solvent-controlled plasmon-assisted surface catalysis reaction of 4-aminothiophenol dimerizing to p, p'-dimercaptoazobenzene on Ag nanoparticles. *Heliyon*. 2019;**5**(4):e01545
- [8] Golubev AA, Khlebtsov BN, Rodriguez RD, Chen Y, Zahn DR. Plasmonic heating plays a dominant role in the plasmon-induced photocatalytic reduction of 4-nitrobenzenethiol. *The Journal of Physical Chemistry C*. 2018;**122**(10):5657-5663
- [9] Tsai M-H, Lin Y-K, Luo S-C. Electrochemical SERS for in situ monitoring the redox states of PEDOT and its potential application in oxidant detection. *ACS Applied Materials and Interfaces*. 2018;**11**(1):1402-1410
- [10] Wu D-Y, Li J-F, Ren B, Tian Z-Q. Electrochemical surface-enhanced Raman spectroscopy of nanostructures. *Chemical Society Reviews*. 2008;**37**(5):1025-1041
- [11] Zhang Q, Wang H. Mechanistic insights on plasmon-driven photocatalytic oxidative coupling of thiophenol derivatives: Evidence for steady-state photoactivated oxygen. *The Journal of Physical Chemistry C*. 2018;**122**(10):5686-5697
- [12] Kim M, Lin M, Son J, Xu H, Nam JM. Hot-electron-mediated photochemical reactions: Principles, recent advances, and challenges. *Advanced Optical Materials*. 2017;**5**(15):1700004
- [13] Kreibitz U, Vollmer M. *Optical Properties of Metal Clusters*. Berlin: Springer; 1995
- [14] Watanabe K, Menzel D, Nilius N, Freund H-J. Photochemistry on metal nanoparticles. *Chemical Reviews*. 2006;**106**(10):4301-4320
- [15] Moskovits M. Surface-enhanced spectroscopy. *Reviews of Modern Physics*. 1985;**57**(3):783
- [16] Alvarez-Puebla R, Liz-Marzán LM, García de Abajo FJ. Light concentration at the nanometer scale. *The Journal of Physical Chemistry Letters*. 2010;**1**(16):2428-2434
- [17] Christopher P, Xin H, Linic S. Visible-light-enhanced catalytic oxidation reactions on plasmonic silver nanostructures. *Nature Chemistry*. 2011;**3**(6):467

- [18] Govorov AO, Zhang H, Demir HV, Gun'ko YK. Photogeneration of hot plasmonic electrons with metal nanocrystals: Quantum description and potential applications. *Nano Today*. 2014;**9**(1):85-101
- [19] Manjavacas A, Liu JG, Kulkarni V, Nordlander P. Plasmon-induced hot carriers in metallic nanoparticles. *ACS Nano*. 2014;**8**(8):7630-7638
- [20] Govorov AO, Zhang H, Gun'ko YK. Theory of photoinjection of hot plasmonic carriers from metal nanostructures into semiconductors and surface molecules. *The Journal of Physical Chemistry C*. 2013;**117**(32):16616-16631
- [21] Gao P, Weaver M, editors. Surface-enhanced Raman-spectroscopy as a vibrational probe of electrochemical reaction-mechanisms-the electroreduction of nitrobenzene. *Journal of the Electrochemical Society*. 1987;**134**(3):c132
- [22] Bello JM, Narayanan VA, Vo-Dinh T. Surface-enhanced Raman scattering interaction of p-aminobenzoic acid on a silver-coated alumina substrate. *Spectrochimica Acta Part A: Molecular Spectroscopy*. 1992;**48**(4):563-567
- [23] You T, Jiang L, Yin P, Shang Y, Zhang D, Guo L, et al. Direct observation of p, p'-dimercaptoazobenzene produced from p-aminothiophenol and p-nitrothiophenol on Cu₂O nanoparticles by surface-enhanced Raman spectroscopy. *Journal of Raman Spectroscopy*. 2014;**45**(1):7-14
- [24] Baia M, Toderas F, Baia L, Popp J, Astilean S. Probing the enhancement mechanisms of SERS with p-aminothiophenol molecules adsorbed on self-assembled gold colloidal nanoparticles. *Chemical Physics Letters*. 2006;**422**(1-3):127-132
- [25] Zhao L-B, Huang Y-F, Liu X-M, Anema JR, Wu D-Y, Ren B, et al. A DFT study on photoinduced surface catalytic coupling reactions on nanostructured silver: Selective formation of azobenzene derivatives from Para-substituted nitrobenzene and aniline. *Physical Chemistry Chemical Physics*. 2012;**14**(37):12919-12929
- [26] Ling Y, Xie WC, Liu GK, Yan RW, Tang J. The discovery of the hydrogen bond from p-Nitrothiophenol by Raman spectroscopy: Guideline for the thioalcohol molecule recognition tool. *Scientific Reports*. 2016;**6**:31981
- [27] Osawa M, Ikeda M. Surface-enhanced infrared absorption of p-nitrobenzoic acid deposited on silver island films: Contributions of electromagnetic and chemical mechanisms. *The Journal of Physical Chemistry*. 1991;**95**(24):9914-9919
- [28] Sun S, Birke RL, Lombardi JR, Leung KP, Genack AZ. Photolysis of p-nitrobenzoic acid on roughened silver surfaces. *The Journal of Physical Chemistry*. 1988;**92**(21):5965-5972
- [29] Roth P, Venkatachalam R, Boerio F. Surface-enhanced Raman scattering from p-nitrobenzoic acid. *The Journal of Chemical Physics*. 1986;**85**(2):1150-1155
- [30] Osawa M, Matsuda N, Yoshii K, Uchida I. Charge transfer resonance Raman process in surface-enhanced Raman scattering from p-aminothiophenol adsorbed on silver: Herzberg-Teller contribution. *The Journal of Physical Chemistry*. 1994;**98**(48):12702-12707
- [31] Hill W, Wehling B. Potential-and pH-dependent surface-enhanced Raman scattering of p-mercapto aniline on silver and gold substrates. *The Journal of Physical Chemistry*. 1993;**97**(37):9451-9455
- [32] Zhou Q, Li XW, Fan Q, Zhang XX, Zheng JW. Charge transfer between

- metal nanoparticles interconnected with a functionalized molecule probed by surface-enhanced Raman spectroscopy. *Angewandte Chemie, International Edition*. 2006;**45**(24):3970-3973
- [33] Wu DY, Liu XM, Huang YF, Ren B, Xu X, Tian ZQ. Surface catalytic coupling reaction of p-Mercaptoaniline linking to silver nanostructures responsible for abnormal SERS enhancement: A DFT study. *The Journal of Physical Chemistry C*. 2009;**113**(42):18212-18222
- [34] Wu D-Y, Zhao L-B, Liu X-M, Huang R, Huang Y-F, Ren B, et al. Photon-driven charge transfer and photocatalysis of p-aminothiophenol in metal nanogaps: A DFT study of SERS. *Chemical Communications*. 2011;**47**(9):2520-2522
- [35] Zhao L-B, Huang R, Huang Y-F, Wu D-Y, Ren B, Tian Z-Q. Photon-driven charge transfer and Herzberg-Teller vibronic coupling mechanism in surface-enhanced Raman scattering of p-aminothiophenol adsorbed on coinage metal surfaces: A density functional theory study. *The Journal of Chemical Physics*. 2011;**135**(13):134707
- [36] Gibson JW, Johnson BR. Density-matrix calculation of surface-enhanced Raman scattering for p-mercaptoaniline on silver nanoshells. *The Journal of Chemical Physics*. 2006;**124**(6):064701
- [37] Sun M, Xu H. Direct visualization of the chemical mechanism in SERRS of 4-Aminothiophenol/metal complexes and metal/4-Aminothiophenol/metal junctions. *ChemPhysChem*. 2009;**10**(2):392-399
- [38] Osawa M, Matsuda N, Yoshii K, Uchida I. Charge-transfer resonance process in surface-enhanced Raman-scattering from p-aminothiophenol adsorbed on silver - Herzberg-Teller contribution. *The Journal of Physical Chemistry*. 1994;**98**(48):12702-12707
- [39] Lombardi JR, Birke RL, Lu T, Xu J. Charge-transfer theory of surface enhanced Raman spectroscopy: Herzberg-Teller contributions. *The Journal of Chemical Physics*. 1986;**84**:4174-4180
- [40] Albrecht AC. On the theory of Raman intensities. *The Journal of Chemical Physics*. 1961;**34**:1476-1484
- [41] Kambhampati P, Child CM, Foster MC, Campion A. On the chemical mechanism of surface enhanced Raman scattering: Experiment and theory. *The Journal of Chemical Physics*. 1998;**108**(12):5013-5026
- [42] Lu Y, Xue G. Study of surface catalytic photochemical reaction by using conventional and Fourier transform surface enhanced Raman scattering. *Applied Surface Science*. 1998;**125**(2):157-162
- [43] Patrino EM, Cometto FP, Paredes-Olivera P. Quantum mechanical investigation of thiourea adsorption on Ag(111) considering electric field and solvent effects. *The Journal of Physical Chemistry. B*. 2004;**108**:15755-15769
- [44] Huang Y-F, Zhu H-P, Liu G-K, Wu D-Y, Ren B, Tian Z-Q. When the signal is not from the original molecule to be detected: Chemical transformation of Para-aminothiophenol on Ag during the SERS measurement. *Journal of the American Chemical Society*. 2010;**132**(27):9244-9246
- [45] Fang Y, Li Y, Xu H, Sun M. Ascertaining p,p'-dimercaptoazobenzene produced from p-aminothiophenol by selective catalytic coupling reaction on silver nanoparticles. *Langmuir*. 2010;**26**(11):7737-7746
- [46] Huang Y, Fang Y, Yang Z, Sun M. Can p,p'-Dimercaptoazobisbenzene Be produced from p-aminothiophenol by surface photochemistry reaction in the junctions of a Ag

- nanoparticle-molecule-Ag (or Au) film? *The Journal of Physical Chemistry C*. 2010;**114**(42):18263-18269
- [47] Tsuji T, Takashima H, Takeuchi H, Egawa T, Konaka S. Molecular structure and torsional potential of trans-azobenzene. A gas electron diffraction study. *Journal of Physical Chemistry A*. 2001;**105**(41):9347-9353
- [48] Briquet L, Vercauteren DP, Perpete EA, Jacquemin D. Is solvated trans-azobenzene twisted or planar? *Chemical Physics Letters*. 2006;**417**(1-3):190-195
- [49] Duan S, Ai Y-J, Hu W, Luo Y. Roles of Plasmonic excitation and protonation on photoreactions of p-Aminobenzenethiol on Ag nanoparticles. *The Journal of Physical Chemistry C*. 2014;**118**(13):6893-6902
- [50] Hill W, Wehling B. Potential-dependent and pH-dependent surface-enhanced Raman-scattering of p-mercaptoaniline on silver and gold substrates. *The Journal of Physical Chemistry*. 1993;**97**(37):9451-9455
- [51] Kim K, Kim KL, Shin KS. Photoreduction of 4,4'-Dimercaptoazobenzene on Ag revealed by Raman scattering spectroscopy. *Langmuir*. 2013;**29**(1):183-190
- [52] Kim K, Choi J-Y, Shin KS. Surface-enhanced Raman scattering of 4-Nitrobenzenethiol and 4-Aminobenzenethiol on silver in icy environments at liquid nitrogen temperature. *The Journal of Physical Chemistry C*. 2014;**118**(21):11397-11403
- [53] Lund H. Cathodic reduction of nitro and related compounds. *Organic Electrochemistry*. 2001;**4**:379-409
- [54] Gorrane A, Corma A, García H. Gold-catalyzed synthesis of aromatic azo compounds from anilines and nitroaromatics. *Science*. 2008;**322**(5908):1661-1664
- [55] Zhu H, Ke X, Yang X, Sarina S, Liu H. Reduction of nitroaromatic compounds on supported gold nanoparticles by visible and ultraviolet light. *Angewandte Chemie, International Edition*. 2010;**49**(50):9657-9661
- [56] Huang W, Zhai H-J, Wang L-S. Probing the interactions of O₂ with small gold cluster anions (Au_n⁻, n= 1– 7): Chemisorption vs physisorption. *Journal of the American Chemical Society*. 2010;**132**(12):4344-4351
- [57] Christopher P, Xin H, Marimuthu A, Linic S. Singular characteristics and unique chemical bond activation mechanisms of photocatalytic reactions on plasmonic nanostructures. *Nature Materials*. 2012;**11**(12):1044
- [58] Linic S, Aslam U, Boerigter C, Morabito M. Photochemical transformations on plasmonic metal nanoparticles. *Nature Materials*. 2015;**14**(6):567
- [59] Tcherniak A, Ha J, Dominguez-Medina S, Slaughter L, Link S. Probing a century old prediction one plasmonic particle at a time. *Nano Letters*. 2010;**10**(4):1398-1404
- [60] Zhao L-B, Zhang M, Huang Y-F, Williams CT, Wu D-Y, Ren B, et al. Theoretical study of plasmon-enhanced surface catalytic coupling reactions of aromatic amines and nitro compounds. *The Journal of Physical Chemistry Letters*. 2014;**5**(7):1259-1266
- [61] Huang Y-F, Zhang M, Zhao L-B, Feng J-M, Wu D-Y, Ren B, et al. Activation of oxygen on gold and silver nanoparticles assisted by surface plasmon resonances. *Angewandte Chemie, International Edition*. 2014;**53**(9):2353-2357
- [62] Goldmann A, Matzdorf R, Theilmann F. Experimental hot-electron

and photohole lifetimes at metal surfaces—What do we know? *Surface Science*. 1998;**414**(1-2):L932-L9L7

[63] Chulkov E, Borisov A, Gauyacq J, Sánchez-Portal D, Silkin V, Zhukov V, et al. Electronic excitations in metals and at metal surfaces. *Chemical Reviews*. 2006;**106**(10):4160-4206

[64] Knoesel E, Hotzel A, Wolf M. Ultrafast dynamics of hot electrons and holes in copper: Excitation, energy relaxation, and transport effects. *Physical Review B*. 1998;**57**(20):12812

IntechOpen